TM Electromagnetic Scattering by a Transparent Wedge with Resistive Faces

Christian Demeterscu, Bair V. Budaev, Constantinos C. Constantinou, and Michel J. Mehler

***Abstract*— The Sommerfeld–Maliuzhinets method is used to calculate the total fields in the interior and exterior regions of an arbitrarily angled resistive wedge. A E-plane wave (TM mode) normally illuminates the two-dimensional resistive wedge. Two spectral functions are introduced to represent the fields in both regions. By imposing the resistive boundary conditions on the wedge faces, a system of coupled functional equations is obtained for the two unknown spectral functions. The functional equations are reduced to singular integral equations for the auxiliary functions. The predictions for a right-angled resistive wedge are shown to be in good agreement with measurements.**

***Index Terms*—Asymptotic analysis, diffraction, electromagnetic scattering.**

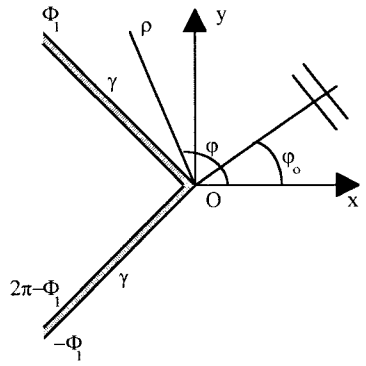

Fig. 1. The resistive wedge geometry and the system of coordinates.

I. Introduction

ELECTROMAGNETIC scattering by hollow wedge structures is of interest in the context of radiowave channel modeling. The scattering around the hollow corners of buildings as well as propagation over pitched roofs are important propagation mechanisms. Rigorous modeling of the transmission through hollow building corners and the associated diffraction phenomena gives the system planners an invaluable method to be used in their coverage prediction tools for the urban environment in cases where radiowave transmission is significant. The real hollow building corners can be simulated at radiowave frequencies by resistive wedges, which are made of two resistive sheets having a common edge and a complex surface resistance. This simplified geometry allows us to construct an accurate solution for the initial scattering problem.

In this paper, the electromagnetic scattering by an arbitrarily angled resistive wedge is presented. The resistive wedge is partially transparent allowing the exterior field to penetrate inside it. Therefore, the problem at hand involves two media. The two walls of the resistive wedge are taken to be identical. The case when the walls are different can be similarly investigated. The total fields in the interior and exterior regions of the resistive wedge are represented in terms of the Sommerfeld–Maliuzhinets integrals [1] involving two unknown spectral functions. By imposing the resistive boundary conditions on the resistive wedge faces, four coupled functional equations are obtained for the two spectral functions. The pole singularities of the two spectral functions are singled out *a priori* by the approach presented in Budaev and Bogy [2], [3]. Then, the problem is reduced to the solution of a singular integral equation for each of the symmetric or anti-symmetric components of the spectral function. The singular integral equation can be subsequently reduced to a Fredholm equation of the second kind. We solve numerically these Fredholm equations and obtain the two spectral functions that satisfy the pole requirement, radiation, and edge conditions. The UTD predictions of the total scattered field by a right-angled resistive wedge are shown to be in good agreement with measurements taken in a controlled laboratory environment.

Manuscript received March 7, 1997; revised July 20, 1998. This work was supported by the British Telecom Laboratories.

C. Demeterscu and C. C. Constantinou are with The University of Birmingham, Birmingham, B15 2TT U.K.

B. V. Budaev is with the University of California at Berkeley, Berkeley, CA 94720 USA.

M. J. Mehler is with the British Telecom Laboratories, Ipswich, IP5 3RE U.K.

Publisher Item Identifier S 0018-926X(99)02220-6.

II. Analysis

The geometry of the problem under consideration, together with the cylindrical polar coordinates employed, is shown in Fig. 1. The resistive wedge has half of the exterior angle equal to Φ_1. A unity amplitude E plane wave normally illuminates the geometry, as depicted in Fig. 1.

The two resistive sheets that form the wedge are identical and have the electrical parameter $\gamma = Z_0/2R_e$, where Z_0 is the free-space impedance and R_e is their complex surface resistivity [4].

The z component of the total electric field in the interior and exterior regions of the resistive wedge, respectively, is represented in terms of the Sommerfeld–Maliuzhinets integrals

[1] as

$$E_z(\rho,\varphi)=\frac{1}{2\pi j}\int_C e^{jk\rho\cos a}S_1(\alpha+\varphi)\,d\alpha,\qquad \text{for } |\varphi|<\Phi_1 \tag{1a}$$

$$E_z(\rho,\varphi)=\frac{1}{2\pi j}\int_C e^{jk\rho\cos\alpha}S_2(\alpha+\varphi-\pi)\,d\alpha,\qquad \text{for } |\varphi-\pi|<\Phi_2 \tag{1b}$$

where Φ_1 is half of the exterior angle of the resistive wedge $\Phi_2=\pi-\Phi_1$, C is the Sommerfeld two loop contour, $S_{1,2}(\alpha)$ are two unknown spectral functions corresponding to the exterior and interior regions of the resistive wedge, respectively, k is the free-space wave number, and (ρ,φ) are the cylindrical polar coordinates shown in Fig. 1. The boundary conditions along the resistive sheets are

$$\frac{\partial}{\rho\partial\varphi}[E_z^+-E_z^-]\pm jk_0\gamma[E_z^++E_z^-]=0,\qquad \text{for } \varphi=\pm\Phi_1 \tag{2a}$$

$$E_z^+-E_z^-=0 \tag{2b}$$

where $E_z^{\pm}$ are the z component of electric fields on the resistive sheets in the exterior and interior regions, respectively. The electric fields given in (1) must satisfy the boundary conditions (2) and the radiation condition. The spectral function $S_1(\alpha)$ corresponding to the exterior region of the resistive wedge, has only one pole with a residue of unity in the strip $|\mathrm{Re}\,\alpha|<\Phi_1$ at $\alpha=\varphi_0$ to correctly recover the incident plane wave (pole requirement). In addition to these requirements, both spectral functions should satisfy the edge condition $S_{1,2}(\alpha)=O(1)$ for $|\mathrm{Im}\,\alpha|\to\infty$.

Substituting the spectral representations of the fields (1) into the boundary conditions (2) and using the inversion formula for the Sommerfeld integrals [5], yields the following system of coupled functional equations for the two unknown spectral functions:

$$\begin{aligned}&(\sin\alpha+\sin\theta)[S_1(\alpha+\Phi_1)-S_2(-\alpha-\Phi_2)]\\&\quad=(\sin\alpha-\sin\theta)[S_2(\alpha-\Phi_2)-S_1(-\alpha+\Phi_1)]+C_1\sin\alpha\end{aligned} \tag{3a}$$

$$S_1(\alpha+\Phi_1)+S_2(-\alpha-\Phi_2)=S_1(-\alpha+\Phi_1)+S_2(\alpha-\Phi_2) \tag{3b}$$

$$\begin{aligned}&(\sin\alpha-\sin\theta)[S_1(\alpha-\Phi_1)-S_2(-\alpha+\Phi_2)]\\&\quad=(\sin\alpha+\sin\theta)[S_2(\alpha+\Phi_2)-S_1(-\alpha-\Phi_1)]+C_2\sin\alpha\end{aligned} \tag{3c}$$

$$S_1(\alpha-\Phi_1)+S_2(-\alpha+\Phi_2)=S_1(-\alpha-\Phi_1)+S_2(\alpha+\Phi_2) \tag{3d}$$

where $\gamma=\sin\theta$, θ is the pseudo-Brewster angle and $C_{1,2}$ are arbitrary constants. For physically realizable passive resistive boundary conditions, the real and imaginary parts of θ must satisfy the inequalities $0<\mathrm{Re}\,\theta\le\pi/2$, $\mathrm{Im}\,\theta\ge 0$. Because the constants $C_{1,2}$ do not have any physical meaning we show that they can be set to zero by a suitable choice of additive constants which may be added to the Sommerfeld integrals (1) without modifying them. We divide (3a) and (3c) by $\sin\alpha$ and take the limit $\mathrm{Im}\,\alpha\to\pm\infty$ to obtain

$$C_1=C_2=S_1(j\infty)+S_1(-j\infty)-S_2(j\infty)-S_2(-j\infty). \tag{4a}$$

The Sommerfeld integrals (1) are invariant under the transformation $S_{1,2}(\alpha)\to S_{1,2}(\alpha)+D_{1,2}$, where $D_{1,2}$ are arbitrary constants. Therefore, applying this transformation in (4a), yields

$$\begin{aligned}C_1=C_2=S_1(j\infty)+S_1(-j\infty)+2D_1-S_2(j\infty)\\-S_2(-j\infty)-2D_2\equiv 0.\end{aligned} \tag{4b}$$

To satisfy the identity (4b), we can choose the arbitrary constants $D_{1,2}$ such as

$$D_{1,2}=-\frac{S_{1,2}(j\infty)+S_{1,2}(-j\infty)}{2} \tag{5}$$

which, therefore, reduces the constants $C_{1,2}$ to zero.

The two spectral functions can be written in terms of their symmetric and antisymmetric components in the form

$$S_{1,2}(\alpha)=S_{1,2}^s(\alpha)+S_{1,2}^a(\alpha) \tag{6}$$

where

$$S_{1,2}^s(\alpha)=\frac{1}{2}[S_{1,2}(\alpha)+S_{1,2}(-\alpha)] \tag{7a}$$

$$S_{1,2}^a(\alpha)=\frac{1}{2}[S_{1,2}(\alpha)-S_{1,2}(-\alpha)]. \tag{7b}$$

Inserting (6) into (3), yields the functional equations satisfied by the antisymmetric components in the form

$$\begin{aligned}&\sin\alpha\big[S_1^a(\alpha+\Phi_1)-S_1^a(\alpha-\Phi_1)\big]+2\sin\theta\big[S_1^a(\alpha+\Phi_1)\\&\quad+S_1^a(\alpha-\Phi_1)\big]+\sin\alpha\big[S_2^a(\alpha+\Phi_2)-S_2^a(\alpha-\Phi_2)\big]=0\end{aligned} \tag{8a}$$

$$\begin{aligned}&\big[S_1^a(\alpha+\Phi_1)+S_1^a(\alpha-\Phi_1)\big]-\big[S_2^a(\alpha+\Phi_2)\\&\quad+S_2^a(\alpha-\Phi_2)\big]=0\end{aligned} \tag{8b}$$

and similarly for the symmetric components

$$\begin{aligned}&\sin\alpha\big[S_1^s(\alpha+\Phi_1)+S_1^s(\alpha-\Phi_1)\big]+2\sin\theta\big[S_1^s(\alpha+\Phi_1)\\&\quad-S_1^s(\alpha-\Phi_1)\big]-\sin\alpha\big[S_2^s(\alpha+\Phi_2)+S_2^s(\alpha-\Phi_2)\big]=0\end{aligned} \tag{9a}$$

$$\begin{aligned}&\big[S_1^s(\alpha+\Phi_1)-S_1^s(\alpha-\Phi_1)\big]+\big[S_2^s(\alpha+\Phi_2)\\&\quad-S_2^s(\alpha-\Phi_2)\big]=0.\end{aligned} \tag{9b}$$

The two systems of (8) and (9) have similar forms and we present in detail only the solution of (8).

The systems of (8) and (9) can be rewritten in the matrix form

$$\begin{bmatrix}S_1^{a,s}(\alpha+\Phi_1)\\S_2^{a,s}(\alpha+\Phi_2)\end{bmatrix}=\begin{bmatrix}\pm R(\alpha) & T(\alpha)\\T(\alpha) & \pm R(\alpha)\end{bmatrix}\begin{bmatrix}S_1^{a,s}(\alpha-\Phi_1)\\S_2^{a,s}(\alpha-\Phi_2)\end{bmatrix} \tag{10}$$

where $R(\alpha)$ and $T(\alpha)$ are the reflection and transmission coefficients, respectively, of a resistive sheet given by Senior and Volakis [4]

$$R(\alpha)=-\frac{\sin\theta}{\sin\alpha+\sin\theta}\quad T(\alpha)=\frac{\sin\alpha}{\sin\alpha+\sin\theta}. \tag{11}$$

Once $S_1^{a,s}(\alpha)$ and $S_2^{a,s}(\alpha)$ have been found in the vertical strips $|\mathrm{Re}\,\alpha| < \Phi_{1,2} + \varepsilon$, $\varepsilon > 0$, respectively, then we can analytically continue them in the entire complex α plane by using (10) iteratively.

Following Budaev and Bogy [2], [3], we write the symmetric and antisymmetric components in the form

$$S_1^{s,a}(\alpha) = \hat{S}_1^{s,a}(\alpha) + \tilde{S}_1^{s,a}(\alpha) \tag{12a}$$

$$S_2^{s,a}(\alpha) = \tilde{S}_2^{s,a}(\alpha) \tag{12b}$$

where $\hat{S}_1^{s,a}(\alpha)$ have the poles of $S_1(\alpha)$ in the strip $|\mathrm{Re}\,\alpha| < \Phi_1$ and $\tilde{S}_1^{s,a}(\alpha)$ are regular functions in the same strip. The function $S_2(\alpha)$ is regular in the vertical strip $|\mathrm{Re}\,\alpha| < \Phi_2$, therefore, the absence of an incident field yields $\hat{S}_2^{s,a}(\alpha) = 0$ in (12b) and $\tilde{S}_2^{s,a}(\alpha)$ are regular in this strip. $S_1(\alpha)$ has only one pole in $|\mathrm{Re}\,\alpha| < \Phi_1$ at $\alpha = \varphi_0$ to correctly recover the incident field. Thus, we can choose the meromorphic functions $\hat{S}_1^{s,a}(\alpha)$ in the form

$$\hat{S}_1^{s,a}(\alpha) = \frac{1}{8}\left[\cot\left(\frac{\alpha - \varphi_0}{4}\right) \mp \cot\left(\frac{\alpha + \varphi_0}{4}\right)\right]. \tag{13}$$

We discuss now only the antisymmetric components $S_{1,2}^a(\alpha)$, the discussion for the symmetric case being similar. The first set of poles of $\hat{S}_1^{s,a}(\alpha)$ located in $|\mathrm{Re}\,\alpha| < \Phi_1$ are at $\alpha = \pm\varphi_0$. Both functions $\hat{S}_1^{s,a}(\alpha)$ have a pole at $\alpha = \varphi_0$ with a residue equal to $1/2$ and, thus, $S_1(\alpha)$, being the sum of the symmetric and antisymmetric components, has a residue equal to unity at this pole, which accounts for the incident field. Each of $\hat{S}_1^{s,a}(\alpha)$ has a pole at $\alpha = -\varphi_0$ with residue equal to $\mp 1/2$, respectively, and, therefore, $S_1(\alpha)$ has a residue equal to zero at this pole.

It is apparent from (10) how the poles of $S_{1,2}^a(\alpha)$ propagate in the complex α plane [2], [3]. If α_p is a pole of $S_{1,2}^a(\alpha)$, then the next set of poles are at $\alpha_p \pm 2\Phi_{1,2}$. The pole of the reflection coefficient in (10) at $\alpha_p = \pm(\pi + \theta)$ gives rise to a set of poles of $S_{1,2}^a(\alpha)$ at $\alpha_p = \pm(\pi + \theta + \Phi_{1,2})$. These are the poles which produce the surface waves, which propagate along the resistive sheet faces.

The residues of the poles corresponding to the geometrical optics (GO) fields are determined by the reflection and transmission coefficients. The residues of the surface wave poles can be written in terms of $S_{1,2}^a(\alpha)$ in the strips $|\mathrm{Re}\,\alpha| < \Phi_{1,2}$, calculated by evaluating the reflection and transmission coefficients in (10) in the limit $\alpha \to \mp(\pi + \theta)$, yielding

$$\begin{aligned}&\mathrm{Res}\, S_{1,2}^a(\alpha)\big|_{\alpha = \mp(\pi+\theta+\Phi_{1,2})} \\ &\quad = \frac{\gamma}{\sqrt{1-\gamma^2}}\left[S_1^a(\Phi_2 + \theta) + S_2^a(\Phi_1 + \theta)\right].\end{aligned} \tag{14}$$

If the arguments of $S_{1,2}^a(\alpha)$ in (14) do not lie in the vertical strips $|\mathrm{Re}\,\alpha| < \Phi_{1,2}$, respectively, then the next recursive step in (10) should be used to bring the arguments in the indicated strips. The poles of $S_1^a(\alpha)$, which might have contributions in the evaluation of the final Sommerfeld integrals (1), are at $\alpha = \varphi_0$ for the exterior incident field, $\alpha = -\varphi_0 \pm 2\Phi_1$ for reflections on the exterior faces of the resistive sheets, $\alpha = \pm(\pi + \theta + \Phi_1)$ for surface waves along the exterior faces of the resistive sheets, and $\alpha = \varphi_0 \mp 2\pi$ for the transmitted field through the resistive wedge. The poles of $S_2^a(\alpha)$, which may be caught inside the loop are at $\alpha = \varphi_0 \mp \pi$ for fields transmitted to the interior of the resistive wedge, $\alpha = -\varphi_0 \pm 2\Phi_2 \pm \pi$ for reflections on the inside faces of the resistive wedge, and $\alpha = \pm(\pi + \theta + \Phi_2)$ for the surface waves propagating on the interior faces of the resistive wedge. For $\Phi_2 < \pi/2$, multiple reflections/transmissions have to be accounted for.

The remaining problem is to find the regular functions $\tilde{S}_{1,2}^a(\alpha)$ in the strips $|\mathrm{Re}\,\alpha| < \Phi_{1,2}$, respectively. We can substitute (12) into (8) to obtain

$$\begin{aligned}&\left[\tilde{S}_1^a(\alpha + \Phi_1) + \tilde{S}_1^a(\alpha - \Phi_1)\right] - \left[\tilde{S}_2^a(\alpha + \Phi_2) + \tilde{S}_2^a(\alpha - \Phi_2)\right] \\ &\quad = R_1(\alpha)\end{aligned} \tag{15a}$$

$$\begin{aligned}&\sin\alpha\left[\tilde{S}_1^a(\alpha + \Phi_1) - \tilde{S}_1^a(\alpha - \Phi_1)\right] + 2\sin\theta\left[\tilde{S}_1^a(\alpha + \Phi_1)\right. \\ &\quad \left. + \tilde{S}_1^a(\alpha - \Phi_1)\right] + \sin\alpha\left[\tilde{S}_2^a(\alpha + \Phi_2) - \tilde{S}_2^a(\alpha + \Phi_2)\right] \\ &\quad = R_2(\alpha)\end{aligned} \tag{15b}$$

where

$$R_1(\alpha) = -\left[\hat{S}_1^a(\alpha + \Phi_1) + \hat{S}_1^a(\alpha - \Phi_1)\right] \tag{16a}$$

$$\begin{aligned}R_2(\alpha) = &-\sin\alpha\left[\hat{S}_1^a(\alpha + \Phi_1) - \hat{S}_1^a(\alpha - \Phi_1)\right] \\ &- 2\sin\theta\left[\hat{S}_1^a(\alpha + \Phi_1) + \hat{S}_1^a(\alpha - \Phi_1)\right]\end{aligned} \tag{16b}$$

where the $R_{1,2}(\alpha)$ terms account for all the poles of the spectral functions in the strips $|\mathrm{Re}\,\alpha| < \Phi_{1,2}$. In (15), by making the following substitutions:

$$X_{1,2}(\alpha) = \tilde{S}_{1,2}^a(\alpha + \Phi_{1,2}) + \tilde{S}_{1,2}^a(\alpha - \Phi_{1,2}) \tag{17}$$

these equations become

$$X_1(\alpha) - X_2(\alpha) = R_1(\alpha) \tag{18a}$$

$$\sin\alpha H(\Phi_1)X_1(\alpha) + 2\gamma X_1(\alpha) + \sin\alpha H(\Phi_2)X_2(\alpha) = R_2(\alpha) \tag{18b}$$

where $H(\Phi)$ is the following integral operator [2]

$$H(\Phi)X(\alpha) = \frac{1}{2j\Phi}\int_{-j\infty}^{j\infty} \frac{X(t)\,dt}{\sin\left[\frac{\pi}{2\Phi}(t - \alpha)\right]}, \quad \mathrm{Re}\,\alpha = 0 \tag{19}$$

whose main property is

$$H(\Phi)\{\tilde{S}(\alpha + \Phi) + \tilde{S}(\alpha - \Phi)\} = \tilde{S}(\alpha + \Phi) - \tilde{S}(\alpha - \Phi) \tag{20}$$

and is valid for any function $\tilde{S}(\alpha)$ holomorphic in the vertical strip $|\mathrm{Re}\,\alpha| < \Phi$.

The functions $\tilde{S}_{1,2}^a(\alpha)$ are regular in the vertical strips $|\mathrm{Re}\,\alpha| < \Phi_{1,2} + \varepsilon$, $\varepsilon > 0$, respectively, therefore, (17) and (18) are defined in the vertical strip $|\mathrm{Re}\,\alpha| < \varepsilon$ where both sides of the equations can be Fourier transformed. Equations (18) are solved numerically in our approach to find $X_{1,2}(\alpha)$. Once these two auxiliary functions have been determined, the functions $\tilde{S}_{1,2}^a(\alpha)$ can be obtained in the regularity strips using the following inverse operators [2], [3]:

$$\tilde{S}_{1,2}^a(\alpha) = \frac{1}{4j\Phi_{1,2}}\int_{-j\infty}^{j\infty} \frac{X_{1,2}(u)\,du}{\cos\left[\frac{\pi}{2\Phi_{1,2}}(u - \alpha)\right]}. \tag{21}$$

It is evident from (21) that the auxiliary functions $X_{1,2}(\alpha)$ need to be known only along the imaginary axis $\mathrm{Re}\,\alpha = 0$,

which is consistent with the condition $\mathrm{Re}\,\alpha = 0$ in (19). Eliminating $X_2(\alpha)$ between the two equations (18) and making the change of variable $\alpha = j\eta$, the following singular integral equation for $X_1(\alpha)$ is obtained:

$$\frac{\tanh\eta}{2}\int_{-\infty}^{\infty} P(t,\eta)x(t)\,dt + 2\frac{\gamma}{\cosh\eta}x(\eta) = r(\eta), \quad \text{for } \mathrm{Im}\,\eta = 0 \tag{22}$$

where the singular kernel $P(t,\eta)$ is

$$P(t,\eta) = \frac{1}{\Phi_1 \sinh\left[\frac{\pi}{2\Phi_1}(t-\eta)\right]} + \frac{1}{\Phi_2 \sinh\left[\frac{\pi}{2\Phi_2}(t-\eta)\right]} \tag{23a}$$

and

$$\begin{aligned} x(\eta) &= X_1(j\eta), \\ r(\eta) &= \frac{1}{\cosh\eta}[R_2(j\eta) + j\sinh\eta H(\Phi_2)R_1(j\eta)]. \end{aligned} \tag{23b}$$

In (22), η is a real variable, therefore the kernel $P(t,\eta)$ has a singularity on the integration path at $t=\eta$. It is worth pointing out that (22) has been normalized by dividing it with $\cosh\eta$. This normalization is important for the accuracy of the numerical results. We use a regularization procedure before discretizing (22). Thus, we reduce (22) to a Fredholm equation of the second kind [6]. The integral equation (22) can be rewritten as

$$Tx(\eta) + \tilde{K}x(\eta) = r(\eta) \tag{24}$$

where T is a singular integral operator defined by

$$Tx(\eta) = \frac{2\gamma}{\cosh\eta}x(\eta) + \tanh\eta\int_{-\infty}^{\infty}\frac{x(t)\,dt}{\Phi_1\sinh\left[\frac{\pi}{2\Phi_1}(t-\eta)\right]} \tag{25}$$

and $\tilde{K}$ is a regular integral operator of the form

$$\tilde{K}x(\eta) = \frac{\tanh\eta}{2}\int_{-\infty}^{\infty} x(t)\left\{\frac{1}{\Phi_2\sinh\left[\frac{\pi}{2\Phi_2}(t-\eta)\right]} - \frac{1}{\Phi_1\sinh\left[\frac{\pi}{2\Phi_1}(t-\eta)\right]}\right\}dt. \tag{26}$$

From the theory of singular integral equations [6], we know that by applying the inverse operator T^{-1} in (24) yields a nonsingular integral equation of the form

$$x(\eta) + T^{-1}\tilde{K}x(\eta) = p(\eta) \equiv T^{-1}r(\eta). \tag{27}$$

The inverse operator T^{-1} is derived in the Appendix in the form

$$T^{-1}p(\eta) = a(\eta)p(\eta) + b(\eta)\int_{-\infty}^{\infty} h(t,\eta)p(t)\,dt \tag{28}$$

where $a(\eta)$, $b(\eta)$ and $h(t,\eta)$ are known functions defined in the Appendix.

We reduce now (27) to a Fredholm equation of the second kind with a regular kernel. We first find the product operator $T^{-1}\tilde{K}$ from (27) by applying T^{-1} on the left of (26) and interchanging the order of integration in the resulting equation to obtain

$$T^{-1}\tilde{K}x(\eta) = a(\eta)\tilde{K}x(\eta) + b(\eta)\int_{-\infty}^{\infty} K_0(u,\eta)x(u)\,du \tag{29}$$

where the regular bounded kernel $K_0(u,\eta)$ is

$$K_0(u,\eta) = \int_{-\infty}^{\infty}\frac{h(t,\eta)\tanh t}{2}\left[\frac{1}{\Phi_2\sinh\left[\frac{\pi}{2\Phi_2}(u-t)\right]} - \frac{1}{\Phi_1\sinh\left[\frac{\pi}{2\Phi_1}(u-t)\right]}\right]dt. \tag{30}$$

Using (29) we can rewrite (27) in the form

$$x(\eta) + \int_{-\infty}^{\infty} K_T(u,\eta)x(u)\,du = p(\eta) \tag{31}$$

where

$$K_T(u,\eta) = \frac{a(\eta)\tanh\eta}{2}\left[\frac{1}{\Phi_2\sinh\left[\frac{\pi}{2\Phi_2}(u-\eta)\right]} - \frac{1}{\Phi_1\sinh\left[\frac{\pi}{2\Phi_1}(u-\eta)\right]}\right] + b(\eta)K_0(u,\eta). \tag{32}$$

Equation (31) is a Fredholm equation of the second kind with a regular kernel that can be directly discretized and solved numerically. Once $x(\eta) = X_1(j\eta)$ has been found along the imaginary axis by solving numerically (31), then using (18a), the second auxiliary function $X_2(\alpha)$ is readily found. $\tilde{S}^a_{1,2}(\alpha)$ are found from (21) in the vertical strips $|\mathrm{Re}\,\alpha| < \Phi_{1,2}$, respectively. Outside these strips, $\tilde{S}^a_{1,2}(\alpha)$ are analytically continued using (15). At this stage, the antisymmetric components $S^a_{1,2}(\alpha)$ are completely determined by (12), (13), and (21).

The symmetric components $\tilde{S}^s_{1,2}(\alpha)$ can be found in a similar way, where the auxiliary functions $Y_{1,2}(\alpha)$ are now

$$Y_{1,2}(\alpha) = \tilde{S}^s_{1,2}(\alpha+\Phi_{1,2}) - \tilde{S}^s_{1,2}(\alpha-\Phi_{1,2}) \tag{33}$$

and the integral operator $U(\Phi)$ for this symmetric case is now

$$U(\Phi)Y(\alpha) = \frac{1}{2j\Phi}\int_{-j\infty}^{j\infty}\cot\left[\frac{\pi}{2\Phi}(t-\alpha)\right]Y(t)\,dt, \quad \mathrm{Re}\,\alpha = 0 \tag{34}$$

which has the property

$$U(\Phi)\{\tilde{S}(\alpha+\Phi) - \tilde{S}(\alpha-\Phi)\} = \tilde{S}(\alpha+\Phi) + \tilde{S}(\alpha-\Phi). \tag{35}$$

The inverse operator, corresponding to $U(\Phi)$ given in (34), is

$$\tilde{S}^s_{1,2}(\alpha) = \frac{j}{4\Phi}\int_{-j\infty}^{j\infty}\tan\left[\frac{\pi}{2\Phi}(t-\alpha)\right]Y_{1,2}(t)\,dt. \tag{36}$$

Substituting (12) into (9) and using the auxiliary functions $Y_{1,2}(\alpha)$ to group the symmetric components of $S_{1,2}(\alpha)$ in the resulting equations we obtain (see (18)–(22) for a similar

approach) the following singular integral equation for $y(\eta) = Y_1(j\eta)$

$$\frac{\tanh\eta}{2}\int_{-\infty}^{\infty} Q(t,\eta)y(t)\,dt + 2\frac{\gamma}{\cosh\eta}y(\eta) = q(\eta), \quad \text{for } \operatorname{Im}\eta = 0 \quad (37)$$

where the singular kernel $Q(t,\eta)$ is

$$Q(t,\eta) = \frac{1}{\Phi_1}\coth\left[\frac{\pi}{2\Phi_1}(t-\eta)\right] + \frac{1}{\Phi_2}\coth\left[\frac{\pi}{2\Phi_2}(t-\eta)\right] \quad (38)$$

and

$$\begin{aligned} q(\eta) = \frac{-1}{\cosh\eta}\{&j\sinh\eta\big[\hat{S}_1^s(j\eta+\Phi_1) + \hat{S}_1^s(j\eta-\Phi_1)\big] \\ &+ 2\gamma\big[\hat{S}_1^s(j\eta+\Phi_1) - \hat{S}_1^s(j\eta-\Phi_1)\big] \\ &+ j\sinh\eta U(\Phi_2)\big[\hat{S}_1^s(j\eta+\Phi_1) - \hat{S}_1^s(j\eta-\Phi_1)\big]\} \end{aligned} \quad (39)$$

with $\hat{S}_1^s(\alpha)$ given in (13).

The singular integral equation (37) is similar to (22) and, therefore, the approach used before to reduce (22) to a Fredholm equation of the second kind with regular kernel can be applied here as well. Once the resulting Fredholm equation is solved numerically for $y(\eta) = Y_1(j\eta)$ then the symmetric components $S_{1,2}^s(\alpha)$ are readily found from (36) and (12).

The spectral functions $S_{1,2}(\alpha)$ are now completely determined in the strips $|\operatorname{Re}\alpha| < \Phi_{1,2}$, respectively, and can be analytically continued in the entire complex α plane using (10).

For the sake of clarity, here we summarize the calculation of the two spectral functions $S_{1,2}(\alpha)$ as follows.

- Step 1 Use (6) to express $S_{1,2}(\alpha)$ in terms of their symmetric and anti-symmetric components $S_{1,2}^{s,a}(\alpha)$.
- Step 2 Use (12) to recast $S_{1,2}^{s,a}(\alpha)$ into $\hat{S}_1^{s,a}(\alpha)$ and $\tilde{S}_{1,2}^{s,a}(\alpha)$ where $\hat{S}_1^{s,a}(\alpha)$ account for the incident field pole while $\tilde{S}_1^{s,a}(\alpha)$ and $\tilde{S}_2^{s,a}(\alpha)$ are regular functions in the strips $|\operatorname{Re}\alpha| < \Phi_{1,2}$, respectively.
- Step 3 Use (13) to calculate $\hat{S}_1^{s,a}(\alpha)$.
- Step 4 Use (17) and (33) to introduce the auxiliary functions $X_{1,2}(\alpha)$ and $Y_{1,2}(\alpha)$ used to calculate $\tilde{S}_{1,2}^a(\alpha)$ and $\tilde{S}_{1,2}^s(\alpha)$, respectively.
- Step 5 Solve numerically the Fredholm equations (31) and that corresponding to (37) for $x(\eta) = X_1(j\eta)$ and $y(\eta) = Y_1(j\eta)$, respectively.
- Step 6 Use the relations between $X_1(\alpha)$ and $X_2(\alpha)$ from (18a) and between $Y_1(\alpha)$ and $Y_2(\alpha)$ from (9) and (33) to find $X_2(\alpha)$ and $Y_2(\alpha)$. At this stage both $X_{1,2}(\alpha)$ and $Y_{1,2}(\alpha)$ are known on the imaginary axis.
- Step 7 Use the inverse operators from (21) and (36) to obtain $\tilde{S}_{1,2}^a(\alpha)$ and $\tilde{S}_{1,2}^s(\alpha)$ in the regularity strips from $X_{1,2}(\alpha)$ and $Y_{1,2}(\alpha)$, respectively. At this stage, the spectral functions $S_{1,2}(\alpha)$ are completely determined in their regularity strips $|\operatorname{Re}\alpha| < \Phi_{1,2}$, respectively.
- Step 8 Use (10) to analytically continue $S_{1,2}(\alpha)$ outside their regularity strips.

By closing the Sommerfeld two-loop contour C in (1) by the two steepest descent paths through the saddle points $\pm\pi$, several poles may be captured inside the resulting loop. These poles give rise to the GO fields and surface waves. The high-frequency approximations of the integrals along the steepest descent paths give rise to diffracted fields in a UTD form.

To validate our predictions, we now present a comparison between the total scattered field by a resistive right-angled wedge and measurements taken in a controlled laboratory environment. In this case, $\Phi_1 = 3\pi/4$ and the exterior UTD diffracted field are

$$E_z^D(\rho,\varphi) = \frac{e^{-jk_0\rho}}{\sqrt{\rho}}D_e(\varphi,\varphi_0,\theta) \quad (40)$$

where the exterior diffraction coefficient $D_e(\varphi,\varphi_0,\theta)$ is given by

$$D_e(\varphi,\varphi_0,\theta) = -\frac{e^{-j\frac{\pi}{4}}}{\sqrt{2\pi k_0}}\left\{S_1(\varphi+\pi) - S_1(\varphi-\pi) - \sum_{k=1}^{5}\frac{\operatorname{Res}_1(k)}{2s_k}\big[1-F_{KP}\big(2k_0\rho s_k^2\big)\big]\right\} \quad (41)$$

where $\operatorname{Res}_1(k)$ are the residues of the poles α_k of $S_1(\alpha+\varphi)$ captured inside the closed loop, $s_k = \cos(\alpha_k/2)$ and $F_{KP}(x)$ is the complex transition function [7]. The explicit expressions for the residues of the GO poles are given by the known reflection and transmission coefficients of (11), while the residues of the surface wave poles are given by (14). Without loss of generality, by symmetry of the geometry in Fig. 1 it is only necessary to consider incidence angles in the interval $\varphi_0 \in [0, 3\pi/4]$. The interior uniform theory of diffraction (UTD) diffracted field has the form

$$E_z^D(\rho,\varphi) = \frac{e^{-jk_0\rho}}{\sqrt{\rho}}D_i(\varphi,\varphi_0,\theta) \quad (42)$$

where the interior diffraction coefficient $D_i(\varphi,\varphi_0,\theta)$ is given by

$$D_i(\varphi,\varphi_0,\theta) = -\frac{e^{-j\frac{\pi}{4}}}{\sqrt{2\pi k_0}}\left\{S_2(\varphi+\pi) - S_2(\varphi-\pi) - \sum_{k=1}^{5}\frac{\operatorname{Res}_2(k)}{2p_k}\big[1-F_{KP}\big(2k_0\rho p_k^2\big)\big]\right\} \quad (43)$$

where $\operatorname{Res}_2(k)$ are the residues of the poles η_k of $S_2(\alpha+\varphi)$ captured inside the closed loop and $p_k = \cos(\eta_k/2)$. In the next section, we compare this UTD form of the total electric field with measurements taken in the laboratory at 30 GHz on a right-angled hollow thin plaster-board wedge. For convenience, we change the reference angle to $\phi = 3\pi/4 - \varphi$, as shown in Fig. 2.

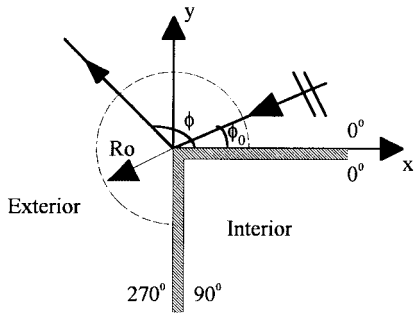

Fig. 2. New system of coordinates.

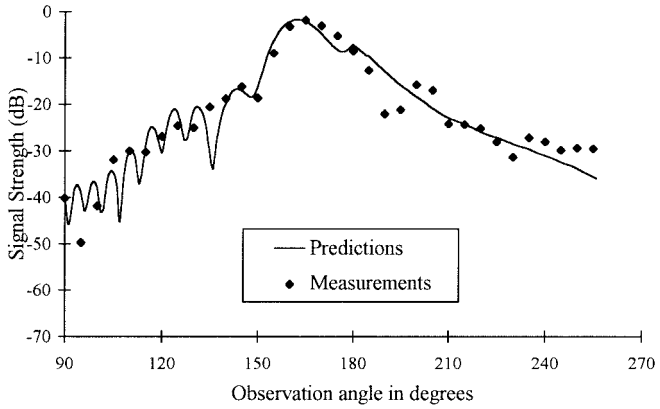

Fig. 3. Exterior region field-strength measurements versus UTD theoretical predictions for right-angled resistive wedge.

III. Numerical Simulations and Experiments

We proceed to establish the validity of the UTD form of the solution presented here through controlled laboratory experiments. We use the Birmingham propagation range, which is a semi-anechoic chamber with a flat aluminum ground plane. The transmitter was a vertically polarized ground-based open-ended WR28 waveguide, fed with a 30-GHz CW constant level signal. A right-angled penetrable dielectric plaster-board hollow wedge was built so that the angle of incidence on the lit face was $\phi_0 = 5°$ and the edge was 1.5 m away from the transmitter. The thickness of the plaster board was 9 mm. The hollow wedge sides were approximately 0.60 m high, one side extending all the way to the transmitter (i.e., was 1.5 m long) and the shadowed side was 1 m long. This geometrical arrangement means that the incident wave was, to a good approximation, a plane wave at the edge and the effects due to the finite size of the resistive wedge are negligible. The receiver was a vertically polarized ground-based standard-gain pyramidal horn antenna with a boreside gain of 18 dBi and a -20 dB beamwidth of $\pm 37°$ in the H plane. The choice of the receiving antenna was dictated by the requirement of detecting the field strength in the deep shadow region of the wedge above the noise floor of our spectrum analyzer (receiver).

In Fig. 3, we present a comparison of the predictions of the new UTD form of the total field against the experimental measurements taken at a distance of $\rho = 10\lambda$ from the edge. The complex relative permitivitty for the plaster was measured to be $\varepsilon_r = 2.2 - j0.181$ using a standard waveguide measurement technique at the chosen experimental frequency. The measurement accuracy was ± 1 dB, while the repeatability of the measurements was ± 0.83 dB (worst case). The receiving antenna was moved along a circular path over 180° in steps of 5°, and its boreside was directed toward the edge of the wedge. The first illuminated quadrant $(0° \leq \phi < 90°)$ and the interior fourth quadrant were not covered, as the receiver support would have interfered with the experiment and the directivity of the horn antenna would have yielded field strength levels near or under the noise floor of our receiver.

Overall, the predictions are in good agreement with the measurements. Our prediction using the UTD form of the scattered field produces a mean error of 0.67 dB and a standard deviation of 4.45 dB. This degree of agreement is justifiable given our measurement accuracy and the fact that we have modeled only very thin dielectric walls as resistive sheets. The discrepancy which occurs around 190° is due to the fact that the thickness of the plaster boards is comparable with the wavelength. Our presented model is suitable for hollow wedges, which have dielectric slab walls sufficiently thin to be modeled as resistive sheets. If the thickness of the dielectric wall increases then the higher order transition boundary conditions should be used for a better simulation of the hollow wedge in which case our method can be expanded to treat the higher order boundary conditions. It was observed that the surface waves were strongly attenuated away from the edge of the resistive wedge, so for most of the practical applications in the context of radiowave propagation, they are negligible. This could not be verified experimentally, as the receiver support structure only allowed us to take measurements up to 260°. Nevertheless, we have verified this through numerical simulations for a range of complex dielectric relative permittivities typical for building materials such as brick and concrete.

We present in Fig. 4 the predicted total field, the GO field, and the UTD diffracted field both in the interior and exterior regions of the right-angled resistive wedge from Fig. 2. A unity E plane wave normally illuminates the right-angled resistive wedge from Fig. 2. The incidence angle is $\phi_0 = 60°$ and the observation point is moving on a complete circle of radius $\rho = 5\lambda$. The relative complex permitivitty of the dielectric from which the resistive sheet is made of is $\varepsilon_r = 2.2 - j0.181$.

Inspection of the data plotted in Fig. 4 reveals that the total field is continuous across the resistive sheets. The diffracted field correctly compensates the GO discontinuities across the incidence/reflection shadow boundaries where the total field is continuous.

IV. Conclusion

In this paper, we presented the diffraction by an arbitrarily angled resistive wedge using the Sommerfeld–Maliuzhinets method. A new UTD diffraction coefficient was derived from a steepest decent uniform asymptotic approximation of the Sommerfeld integrals for the right-angled resistive wedge. This UTD form of the total field was compared with measurements taken in a controlled laboratory environment and good agreement was obtained throughout.

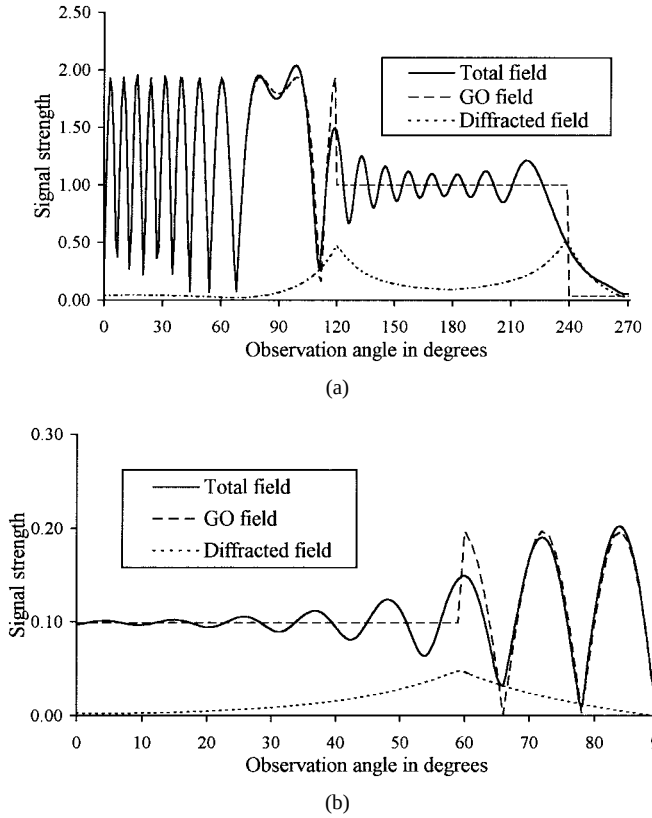

Fig. 4. (a) Exterior and (b) interior fields for a right-angled resistive wedge.

We have identified the existence of surface waves, which are exponentially attenuated both with distance from the edge of the wedge and with increasing angular separation from the faces of the wedge. The excitation of these surface waves is sensitive to the electrical parameters of the dielectric material from which the resistive sheets are composed. For most practical applications, especially in the urban mobile radio propagation prediction programs of current interest, these waves have been found to be negligible through numerical simulations. The critical factor in making reliable predictions seems to be the accuracy with which the boundary value problem is modeled on the dielectric hollow wedge walls and, in particular, on the shadowed face. The experimental results were taken for a wall thickness of 0.9-free-space wavelengths and were found to be in good agreement with the analysis. When the thickness of the dielectric slabs, which form the walls of the hollow wedge increases, higher order transition boundary conditions are likely to be required for a better simulation of the actual hollow wedge.

APPENDIX

In this Appendix, we derive the expression of the inverse operator T^{-1}. The operator inversion problem can be stated as follows: find the solution $X(\alpha)$ of

$$Tx(\eta) = p(\eta) \tag{A.1}$$

providing that $p(\eta)$ is a known function decaying at $|\mathrm{Re}\,\eta| \to \infty$ and the operator T is given in (25). In other words we want to express $x(\eta)$ as $x(\eta) = T^{-1}p(\eta)$. We use the notations $x(\eta) = X(j\eta)$ and $\alpha = j\eta$ in order to express $X(\alpha)$ in the form

$$X(\alpha) = S(\alpha + \Phi_1) + S(\alpha - \Phi_1) \tag{A.2}$$

where $S(\alpha)$ is an unknown function holomorphic in the vertical strip $|\mathrm{Re}\,\alpha| < \Phi_1$. Inserting (A.2) into (A.1) and using (19) and (20) yields

$$TX(\alpha) \equiv \frac{2}{\cos\alpha}[(\sin\alpha + \gamma)S(\alpha + \Phi_1) - (\sin\alpha - \gamma)S(\alpha - \Phi_1)] = P(\alpha) \tag{A.3}$$

where $P(\alpha) \equiv P(j\eta) = p(\eta)$. Equation (A.3) is a first-order difference equation for the unknown function $S(\alpha)$. To solve it we follow Maliuzhinets' approach [1] and express $S(\alpha)$ in the form

$$S(\alpha) = \Psi(\alpha)\sigma(\alpha) \tag{A.4}$$

where $\Psi(\alpha)$ is the bounded solution of the homogeneous equation corresponding to (A.3) of the form

$$\Psi(\alpha) = \exp\left\{\frac{j}{4\Phi_1}\int_{-j\infty}^{j\infty}\tan\left[\frac{(\nu-\alpha)\pi}{2\Phi_1}\right]\ln g(\nu)\,d\nu\right\} \qquad |\mathrm{Re}\,\alpha| < \Phi_1 \tag{A.5}$$

where

$$g(\alpha) = \frac{\Psi(\alpha + \Phi_1)}{\Psi(\alpha - \Phi_1)} = \frac{\sin\alpha - \gamma}{\sin\alpha + \gamma} \tag{A.6}$$

and $\sigma(\alpha)$ satisfies the following inhomogeneous first-order difference equation

$$\sigma(\alpha + \Phi_1) - \sigma(\alpha - \Phi_1) = \frac{P(\alpha)\cos\alpha}{2\Psi(\alpha + \Phi_1)(\sin\alpha + \gamma)}. \tag{A.7}$$

Using the Fourier transform method [1], we can find the solution $\sigma(\alpha)$ of (A,7) in the form

$$\sigma(\alpha) = \frac{j}{8\Phi_1}\int_{-j\infty}^{j\infty}\frac{P(z)\cos z}{\Psi(z + \Phi_1)(\sin z + \gamma)}\tan\left[\frac{(z-\alpha)\pi}{2\Phi_1}\right]dz \qquad |\mathrm{Re}\,\alpha| < \Phi_1. \tag{A.8}$$

Outside the regularity strip $|\mathrm{Re}\,\alpha| < \Phi_1$, the functions $\Psi(\alpha)$ and $\sigma(\alpha)$ are analytically continued by (A.6) and (A.7), respectively. Inserting (A.8), (A.5), and (A.4) into (A.2) yields the inverse operator T^{-1} in the form

$$x(\eta) = T^{-1}p(\eta) \equiv a(\eta)p(\eta) + b(\eta)\int_{-\infty}^{\infty}h(t,\eta)p(t)\,dt \tag{A.9}$$

with

$$a(\eta) = \frac{j\cosh\eta}{2(\sinh\eta + j\gamma)}, \quad b(\eta) = \frac{1}{4\Phi_1}\frac{\Psi(j\eta + \Phi_1)\sinh\eta}{(\sinh\eta + j\gamma)} \tag{A.10}$$

$$h(t,\eta) = \frac{\coth\left[\frac{\pi}{2\Phi_1}(t-\eta)\right]\cosh t}{\Psi(jt + \Phi_1)(j\gamma - \sinh t)}. \tag{A.11}$$

REFERENCES

[1] G. D. Maliuzhinets, "Excitation, reflection and emission of surface waves from a wedge with given face impedances," *Sov. Phys. Doklady*, vol. 3, pp. 752–755, 1958.

[2] B. V. Budaev and D. B. Bogy, "Rayleigh wave scattering by a wedge," *Wave Motion*, vol. 22, pp. 239–257, 1995.

[3] _____, "Rayleigh wave scattering by a wedge 2," *Wave Motion*, vol. 24, pp. 307–314, 1996.

[4] T. B. A. Senior and J. L. Volakis, *Approximate Boundary Conditions in Electromagnetics*. London, U.K.: IEE Press, 1995, pp. 53–76.

[5] G. D. Maliuzhinets, "Inversion formula for the Sommerfeld integral," *Sov. Phys. Doklady*, vol. 3, pp. 52–56, 1958.

[6] N. I. Muskhelishvili, *Singular Integral Equations*. Groningen, The Netherlands: Noordhoff, 1953.

[7] R. G. Kouyoumjian and P. H. Pathak, "A uniform geometrical theory of diffraction for an edge in a perfectly conducting surface," *Proc. IEEE*, vol. 62, pp. 1448–1461, Nov. 1974.

Cristian Demeterscu received the B.Sc. degree from the University of Craiova, Romania, and the Ph.D. degree from the University of Birmingham, U.K., both in electrical engineering, in 1993 and 1997, respectively.

In 1997, he joined Bell Laboratories, Lucent Technologies, Swindon, U.K., where he is working as a Systems Network Researcher in the GSM and UMTS packet networks group. He was involved in the performance evaluation and implementation of the GSM phase 2+ packet network (GPRS). His research interests include control and scheduling algorithms for packet networks, coding and ARQ schemes for radio link protocols, and asymptotic high-frequency methods for electromagnetic fields.

Bair V. Budaev was born in Burjat-Mongolian, Republic of the Soviet Union, on May 20, 1954. He received he Diploma and Candidate of Sciences degrees from the Leningrad State University in 1976 and 1979, respectively, and the Doctor of Sciences degree from the Russian Academy of Sciences, St. Petersburg (Leningrad), in 1995.

He has taught mathematics at the Leningrad Military School of Civil Engineering, the Leningrad Polytechnical Institute, and the Leningrad State University. In 1984 he joined the Leningrad Branch of the Steklov Mathematical Institute, where he worked on problems of wave propagation and diffraction. Since 1995 he has been visiting the University of California at Berkeley, where he continues his research and teaching practice.

Constantinos C. Constantinou received the Bachelor's and Ph.D. degrees in electronic and communications engineering from the University of Birmingham, U.K., in 1987 and 1991, respectively.

In 1989, he joined the Faculty of the School of Electronic and Electrical Engineering as a full-time Lecturer and, subsequently, as a Senior Lecturer. His research interests include optics, electromagnetic theory, electromagnetic scattering and diffraction, electromagnetic measurement, radio wave propagation modeling, and mobile radio. He currently heads the radio wave propagation research activity in the Communications Engineering Research Group.

Michel J. Mehler received the B.S. (electronic and communications engineering) and Ph.D. (electromagnetics) degrees, both from the University of Birmingham, U.K., in 1980 and 1986, respectively.

He then joined BT Research Laboratories, Ipswich, U.K., and spent a period of four years working on most aspects of reflector antenna design. He joined the University of Birmingham, U.K., as a Lecturer and then a Senior Lecturer specializing in electromagnetics. In 1989 he rejoined BT Laboratories to head the Radio Science Group. He currently manages the Corporate Research Program in the area of networks technology at BT Laboratories, with particular responsibility for the optics, radio, and switching. His research experience has been in the fields of antenna synthesis and analysis, radio wave propagation, and electromagnetic scattering. He also has considerable experience in the field of electromagnetic measurement techniques.